Check for updates

JGR Atmospheres

RESEARCH ARTICLE
10.1029/2021JD035607

Spatial Variation of Surface O_3 Responses to Drought Over the Contiguous United States During Summertime: Role of Precursor Emissions and Ozone Chemistry

Wei Li[1], Yuxuan Wang[1], James Flynn[1], Robert J. Griffin[2], Fangzhou Guo[2], and Jordan L. Schnell[3]

[1]Department of Earth and Atmospheric Sciences, University of Houston, Houston, TX, USA, [2]Department of Civil and Environmental Engineering, Rice University, Houston, TX, USA, [3]Cooperative Institute for Research in Environmental Sciences, University of Colorado Boulder NOAA/Global Systems Laboratory, Boulder, CO, USA

Key Points:

- O_3 responses to drought display an east-west discrepancy in the contiguous US: higher enhancement in the southeast yet decrease in the west
- The decrease of O_3 in California is due to the up to 24% reduction of the O_3 production rate (PO_3) caused by the decrease of isoprene
- The increase of isoprene in the southeast causes an increase of PO_3 by up to 33%, accounting for more than half of the O_3 enhancement

Supporting Information:

Supporting Information may be found in the online version of this article.

Correspondence to:

Y. Wang,
ywang246@central.uh.edu

Citation:

Li, W., Wang, Y., Flynn, J., Griffin, R. J., Guo, F., & Schnell, J. L. (2022). Spatial variation of surface O_3 responses to drought over the contiguous United States during summertime: Role of precursor emissions and ozone chemistry. *Journal of Geophysical Research: Atmospheres*, *127*, e2021JD035607. https://doi.org/10.1029/2021JD035607

Received 26 JUL 2021
Accepted 23 DEC 2021

© 2022. American Geophysical Union. All Rights Reserved.

Abstract Drought is an extreme weather and climate event that has been shown to cause the worsening of ozone (O_3) air pollution. Using 15-year (2005–2019) surface O_3 observations and weekly US Drought Monitor (USDM) indices, this study estimated that summertime US-mean surface O_3 increased by 1.47 ppb per USDM level. It is revealed that O_3 responses to drought display a spatial east-west variation: higher O_3 enhancement in the Southeast (2.24 ppb/USDM), and no significant change or even a decrease in the west (e.g., −0.06 ppb/USDM in California). The diurnal changes of O_3 with drought also show an opposite pattern between the Southeast and California. Formaldehyde (HCHO) and nitrogen dioxide (NO_2) column, two satellite-based O_3 precursors proxies, show an increasing rate of 0.41×10^{15} molec/cm^2/USDM and 0.03×10^{15} molec/cm^2/USDM in the Southeast, respectively, while these rates are not statistically significant in California. We explained this spatial discrepancy from the perspective of O_3 chemistry by applying a zero-dimensional model at the sites with long-term observations in California and Georgia. Isoprene concentrations decreased by ∼37% under exceptional drought in California causing a reduction of O_3 production (PO_3) by ∼23.7% during daytime. On the contrary, isoprene increased by ∼41% in Georgia inducing a consequent increase of PO_3 by ∼33.4% which accounts for more than half of the O_3 enhancement. This study reveals the key role of biogenic isoprene on ozone chemistry under drought conditions.

1. Introduction

Drought, as a recurring hydroclimate extreme, can strike the contiguous United States (CONUS) with various severity, duration, and frequency (Chen et al., 2019). Drought brings prolonged dry conditions of the atmosphere and the land, often accompanied by high temperatures. These conditions not only change atmospheric processing mechanisms of chemical constituents, such as chemistry and transport, but also perturb the land-atmosphere exchange of chemical species. Therefore, droughts potentially impose large changes on the abundance of reactive species in the atmosphere, such as ozone (O_3), a criteria air pollutant detrimental to human and ecosystem health.

Most of the prior investigations of O_3 changes under drought are case studies of a given drought period over a specific region (Abeleira & Farmer, 2017; Demetillo et al., 2019; Huang et al., 2016; Solberg et al., 2008; Zhang & Wang, 2016). For example, Zhang and Wang (2016) attributed high O_3 extremes in October 2010 over the southeastern US to dry and warm weather under drought. Demetillo et al. (2019) showed summertime O_3 decreased slightly in California during the severe drought period from 2011 to 2015. These case studies reveal that the magnitude and sign of the drought-O_3 relationship differ by region and season. Long-term analyses of drought impact on atmospheric composition are less common. Using *in situ* O_3 measurements at surface sites and a 1-month standardized precipitation evapotranspiration index (SPEI) as an indicator of drought severity, Wang et al. (2017) quantified that growing-season (March–October) droughts in the CONUS over the recent two-and-half decades (1990–2014) caused an average increase of 3.5 ppb in surface O_3. As drought can develop rapidly and change severity within a month (Chen et al., 2019; Otkin et al., 2018), this study improves upon Wang et al. (2017) by using weekly drought indices and quantifying O_3 responses to drought severity.

Drought impacts on surface O_3 can result from different processes and mechanisms, including the emission of biogenic sources of O_3 precursors [e.g., biogenic volatile organic compounds (BVOCs) and soil nitrogen oxides ($NO_x = NO + NO_2$)], chemical production and loss in the atmosphere, dry and wet deposition of O_3 and precursors,

and transport and mixing related to abnormal atmospheric circulations during drought (Demetillo et al., 2019; Horton et al., 2014; Huang et al., 2016; Jiang et al., 2018; Kavassalis & Murphy, 2017; Lin et al., 2019; Naimark et al., 2021; Wang et al., 2017). For example, both laboratory and field measurements have shown that biogenic emissions of isoprene—the dominant BVOC species and a key O_3 precursor—will increase at the initial stage of drought development primarily due to temperature stimulus but drop eventually under prolonged severe drought limited by soil water availability (Brilli et al., 2007; Pegoraro et al., 2005; Potosnak et al., 2014). Drought-induced changes in isoprene are expected to cause nonlinear responses in O_3 chemistry under drought conditions. When NO_x concentrations are low, O_3 production changes little with increasing VOCs but increases with increasing NO_x as NO facilitates radical recycling. This is known as the NO_x-limited regime. When NO_x concentrations are high, O_3 production increases with increasing VOCs but decreases with increasing NO_x as NO_2 terminates radical propagation. This is called the VOC-limited regime. Thus, the resulting changes of O_3 production under drought depend not only on the sign of the drought-isoprene and drought-NO_x relationships but also on the O_3 formation regimes, which is expected to be region-specific (Duncan et al., 2010; Jin et al., 2018).

This study aims to characterize regional differences in surface O_3 responses to drought in the CONUS and to understand the role of O_3 chemistry in causing such differences. We used gridded O_3 measurements from long-term surface monitoring networks and weekly released US Drought Monitor (USDM) maps to explore the drought-O_3 relationships. These datasets provide better spatial coverage and finer temporal scales than previous studies of O_3 responses to drought (e.g., Wang et al., 2017). The study period is 2005–2019 with a focus on summer when O_3 chemistry is most active. We first examined how the spatial distributions of surface O_3 and its precursors would change with drought over the CONUS. Then, a zero-dimensional model was applied to help explain the spatial pattern from the perspective of drought perturbations on tropospheric O_3 chemistry.

2. Data and Methods

2.1. Drought Indicator

Many indices have been developed since 1916 to indicate dryness levels (Heim, 2002). Based on the location and sector applied, these indices consider different factors, such as precipitation, temperature, evapotranspiration, and vegetation health (McKee et al., 1993; Vicente-Serrano et al., 2010). Here we selected the USDM index because it is a composite product synthesizing not only objective indicators but also inputs of regional and local experts around the country (Svoboda et al., 2002). USDM maps have been released every week from 2000 to the present. There are five dryness categories in the map, labeled Abnormally Dry (D0), Moderate (D1), Severe (D2), Extreme (D3), and Exceptional (D4) Drought. The USDM website (https://droughtmonitor.unl.edu/) provides the shapefiles of the polygons under each of the five drought categories. We downloaded, rasterized, and converted these weekly shapefiles to $0.5° \times 0.5°$ gridded data with 0–4 indicating drought severity from D0 to D4, respectively, and −1 indicating non-drought (wet and normal) conditions (ND). There are 196 weeks in total during our study period of 2005–2019 summers (June, July, August; JJA). Hereafter, we used Δ to denote the changes from ND for the discussed variables unless noted otherwise.

2.2. Atmospheric Composition Data

To expand the spatial coverage, we adopted and expanded the gridded hourly O_3 data ($1° \times 1°$) initially created by Schnell et al., (2014), which aggregates several observation networks of O_3 measurements available from 2005 to 2019. The networks include US Environmental Protection Agency's (EPA) Air Quality System (AQS), Clean Air Status and Trends Network (CASTNET), and Environment Canada's National Air Pollution Surveillance Program (NAPS).

To examine the concurrent changes of isoprene and NO_x emissions, we applied the Ozone Monitoring Instrument (OMI) level-3 daily total formaldehyde (ΩHCHO) and tropospheric nitrogen dioxide (ΩNO_2) column data (https://acdisc.gesdisc.eosdis.nasa.gov/data/Aura_OMI_Level3). Since HCHO is a high-yield oxidation product of isoprene, ΩHCHO is commonly used as a space-based indicator of isoprene emissions (Kaiser et al., 2018; Zhu et al., 2017). OMI was launched in 2004 with a local overpass time around 1:30 p.m. The spatial resolution is $0.1° \times 0.1°$ for ΩHCHO and $0.25° \times 0.25°$ for ΩNO_2. The values below the OMI detection limit of 1.5×10^{15} molec/cm^2 were filtered for both parameters (Duncan et al., 2010; Jin et al., 2018). All the spatial data were

regridded to match the USDM resolution of 0.5° × 0.5°. We first calculated the weekly mean of each variable (i.e., O_3, ΩHCHO, and ΩNO_2) and then averaging the weekly means onto each USDM level.

2.3. LaRC Zero-Dimensional Model

We used NASA Langley Research Center (LaRC) photochemical zero-dimensional model to investigate how O_3 chemistry changes under drought conditions. Details of the model and chemical reactions were described by Crawford et al. (1999) and Olson et al. (2006). It is widely used to examine O_3 photochemistry and has comparable performance with other box models (Flynn et al., 2010; Guo et al., 2021; Schroeder et al., 2017). We ran the model in a time-dependent mode, in which the model run continues until all the radical species reach diurnal equilibrium. The model was constrained by observations of trace gases including NO, NO_x, methane, ethane, propane, ethene, isoprene, and other non-methane hydrocarbons (NMHCs), and by meteorological parameters such as temperature (T), dew point temperature (T_d), solar radiation, and pressure. All these data were downloaded from EPA Data Mart (https://aqs.epa.gov/aqsweb/documents/data_api.html) for the AQS sites used to constrain the model (see Section 3.3). The model can output VOC reactivity (VOCR), rates of instantaneous O_x ($O_x \equiv O_3 + NO_2$) formation (FO_3), destruction (DO_3), and net production ($PO_3 = FO_3 - DO_3$), as well as the reaction rates contributing to FO_3 and DO_3. NO_2 has a high observational bias due to the monitoring method (Lamsal et al., 2008). Here we assume this bias has little effect on the results as we compare the relative changes from non-drought conditions. The details of the selected AQS sites for the model simulation are listed in Table S1 in Supporting Information S1. We averaged the input data within each USDM category before the model run to reduce noises and focus on regional drought characteristics.

3. Results

3.1. Spatial Distributions of O_3 Response to Drought

Figure 1a shows the occurrence frequency of drought at each USDM level over the study period. The western and southern states are more prone to drought than the northeastern states, especially for D3–D4. Figure 1b shows the maximum daily 8-hr average (MDA8) O_3 mixing ratios at ND and ΔO_3 for D0–D4. Under non-drought conditions (ND), MDA8 O_3 is higher in the western states, reflecting the average spatial distributions of summertime O_3. Under droughts, the southeastern states have the highest ΔO_3 of up to ~15 ppb. The states on the Great Plain show a smaller enhancement of about 5 ppb, whereas MDA8 ozone shows a decrease during droughts over parts of California and Nevada. The decrease in ΔO_3 from east to west clearly reveals the spatial east-west contrast in the O_3 response to drought.

To reduce the potential sampling bias caused by the different number of grids under each USDM level (cf. Figure 1a), we first quantified the O_3 changes only for those grids with all USDM levels occurring during our study period (grid number N = 1,067). Figure 1c displays O_3 distributions by USDM over these grids. As the grid restriction substantially limits the areas considered, the same analysis using all the grids under each USDM level is shown in Figure S1 in Supporting Information S1 and similar results were found as the limited-grid approach. As Figure 1c shows, O_3 gradually increases from ND to D4 in almost all aspects of the statistical distribution (e.g., mean, median, four quartiles). Compared with ND, the USDM-mean MDA8 O_3 increases by approximately 2.29, 4.17, 5.32, 6.56, and 7.55 ppb under D0-D4 respectively, with an average rate of 1.47 ppb/USDM. It is noteworthy that the rate of O_3 increase becomes slower at higher USDM levels (D3 and D4), indicating a nonlinear change of O_3 with drought severity. Although droughts are temporally irregular events, summertime O_3 in the CONUS has a decreasing trend in the past two decades because of the reduction of anthropogenic emissions (Simon et al., 2015; Yan et al., 2018). To examine whether this trend would influence the O_3 response to drought, we detrended O_3 by removing the 7-year moving average from the raw O_3 data in the same week of each year (Wang et al., 2017) and used the detrended O_3 data to reproduce the O_3 distributions by USDM levels in Figure 1d. The detrend also reduces the seasonal impacts caused by the uneven distributions of each USDM level among the summer months. As a result, the detrended data have similar O_3 enhancements and change rate (1.41 ppb/USDM) as the original data. Similar results were also found if the 5- and 9-year moving average were used to detrend the data (Figure S2 in Supporting Information S1), which confirms the O_3 enhancement by drought despite decreasing anthropogenic emissions. This is consistent with the conclusions from Wang et al. (2017) that natural processes play a more important role in causing O_3 increase during drought.

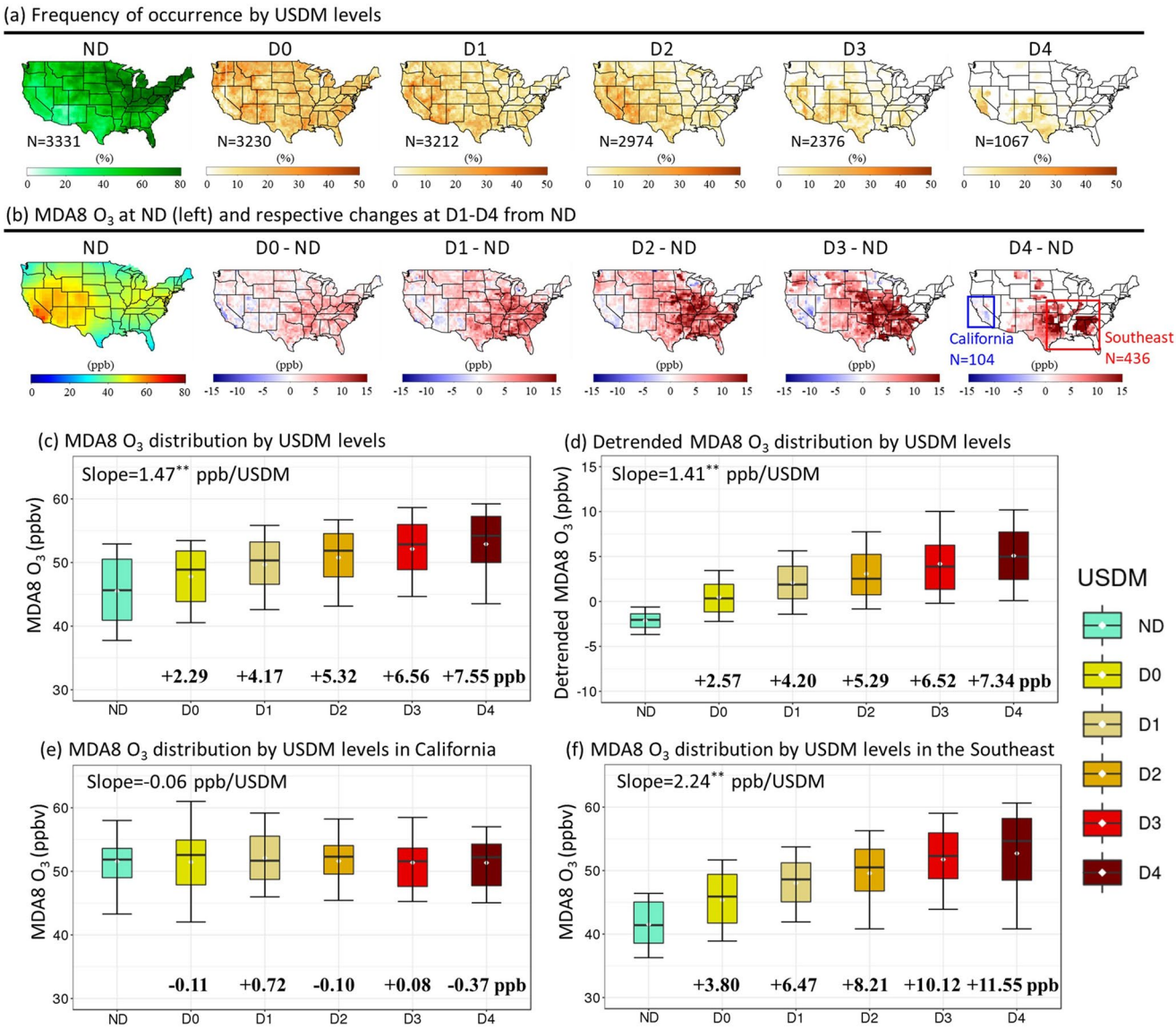

Figure 1. (a) Maps of the frequency of occurrence of each US Drought Monitor (USDM) level during the study period. The number of grids is denoted by *N*. (b) Maps of mean MDA8 O_3 at non-drought (ND) (first column) and ΔO_3 under other USDM levels (second–sixth columns). Blue and red boxes delineate the regions of California and the southeast, while *N* shows the number of grids therein (c and d) Boxplots for raw and detrended MDA8 O_3 in the grids in which all six dryness levels occurred ($N = 1{,}067$), respectively (e and f) Boxplots of the distribution of MDA8 O_3 changes with USDM in California (e) and the southeast (f). The upper and lower whiskers of the boxplots represent the ninth and first quantile, respectively. The numbers below each box show the mixing ratio changes from ND. Slopes indicate the MDA8 changes per USDM using a least-square linear fit of the USDM-mean MDA8. Double star marks denote P-values of the linear fit smaller than 0.01.

To better characterize the abovementioned east-west contrast in the response of O_3 to drought, we separately analyzed two regions: California (33°–42°N, 114°–124°W) and the southeast (26.75°–40°N, 79°–99°W). In each region, only those grids with all D0–D4 occurring and no missing O_3 data (Figure 1b) were used to calculate the regional-mean MDA8 O_3 at each drought level. The distributions of MDA8 O_3 in each region are displayed in Figures 1e and 1f. Their mean and standard deviation values are listed in Table S2 in Supporting Information S1. The O_3 means in California increase first from ND to D1 and then drop from D1 to D4, leading to a statistically insignificant decrease rate of −0.06 ppb/USDM. On the contrary, average O_3 values in the Southeast gradually increase from ND to D4, with a much higher and statistically significant rate of 2.24 ppb/USDM. This further consolidates the east-west disparity of O_3 response to drought.

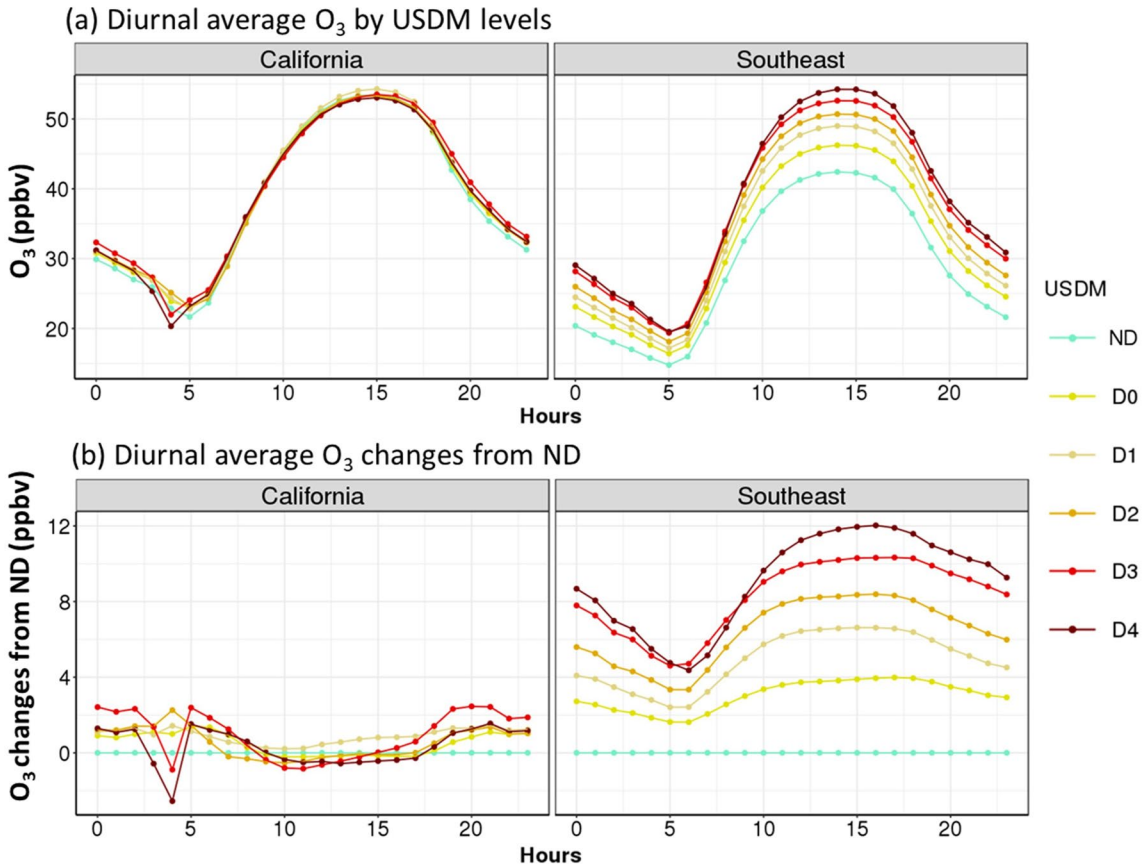

Figure 2. Diurnal mean of O_3 mixing ratio by US Drought Monitor (a) and their differences from non-drought (b) in two regions.

In addition to MDA8 O_3, we further investigated the diurnal pattern of O_3 and ΔO_3 by USDM in each region (Figure 2) in order to obtain more insight into the processes linking drought with O_3 other than at the peak hours. The diurnal cycle of O_3 at all USDM levels in each region resembles the typical O_3 cycle with troughs in the early morning (4:00–6:00) and peaks in the early afternoon (13:00–15:00). The between-USDM difference of O_3 can be clearly seen in the southeast (Figure 2b), yet it is not so obvious in California (Figure 2a). The diurnal patterns of ΔO_3 in Figure 2b further illustrate the regional differences by USDM. In the morning (07:00–11:00), the southeast area has a fast increase of ΔO_3, while in California, ΔO_3 is stable at ~0.8 ppb under D0–D1 and about 0.2–0.4 ppb below normal (i.e., ND level) under D2–D4. In the afternoon (12:00–16:00), ΔO_3 reaches its peak of approximately 4–12 ppb in the southeast but is at the lowest of ~ –0.7 ppb under D2–D4 in California. From the late afternoon to early morning (17:00–6:00), ΔO_3 gradually drops to its minimum values in the southeast, while it stays steady between ~0.5 and ~1.7 ppb in California. The abnormally low ΔO_3 in California at 4:00 under D3 and D4 is caused by extremely low values in some coastal grids, which are outside two times the standard deviation of ~3 ppb during other hours.

Overall, the diurnal changes of ΔO_3 also show an opposite pattern between the southeast and California, especially during the afternoon hours when O_3 quickly builds up through photochemical reactions. Because changes in dry deposition are reported to cause higher O_3 under drought (Huang et al., 2016; Kavassalis & Murphy, 2017; Lin et al., 2019), the opposite behaviors of ΔO_3 between the two regions for both peak O_3 (i.e., MDA8) and diurnal patterns indicate dry deposition may not be the only factor at play. We hypothesize that O_3 chemistry is an important process causing the east-west ΔO_3 disparity under drought. To verify this hypothesis, we limited our scope to understanding how the O_3 chemistry changes with drought in each region by examining O_3 precursors in the next section.

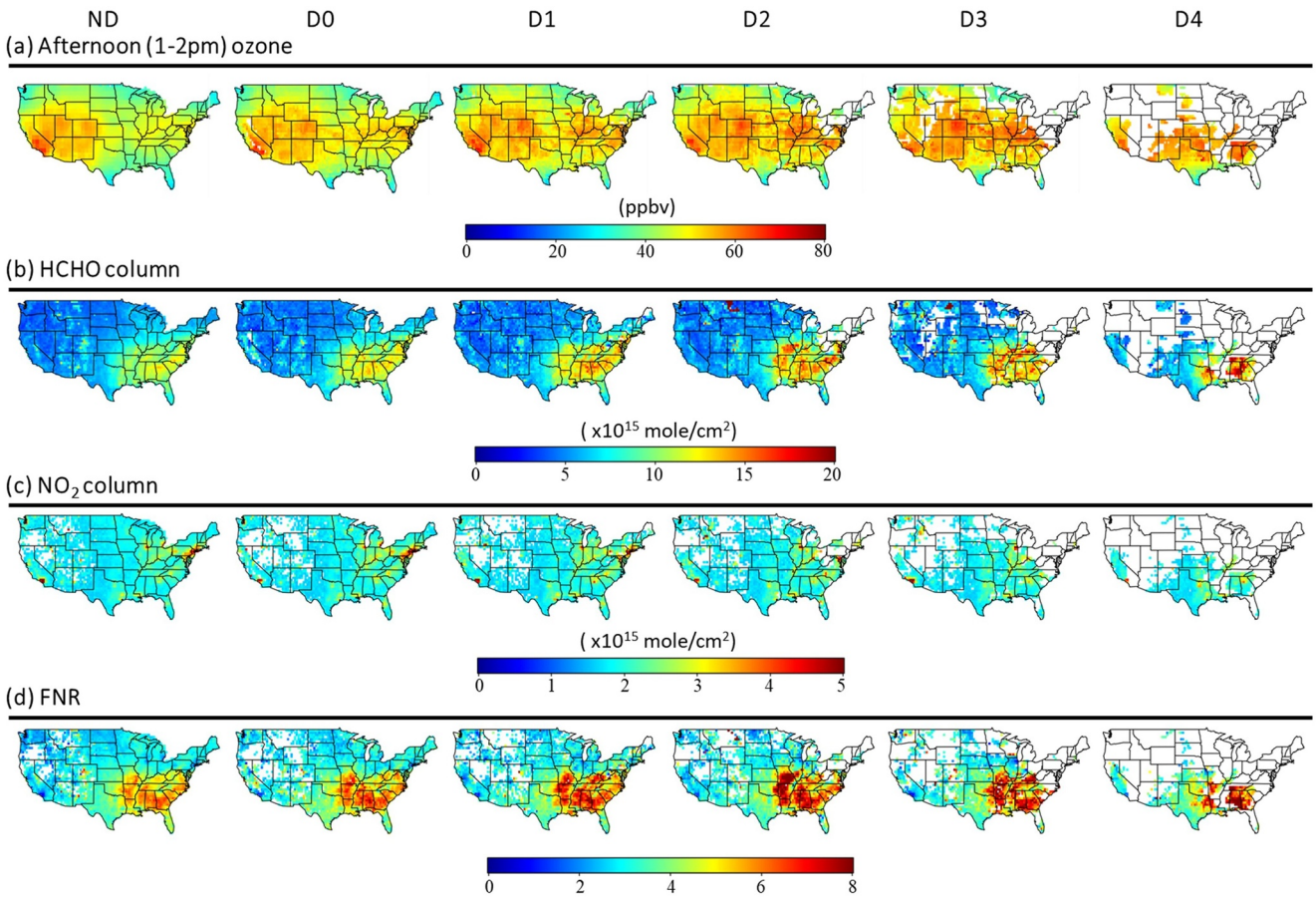

Figure 3. Maps of early afternoon (13:00–14:00) O_3 (a), ΩHCHO (b), ΩNO_2 (c), and FNR (d; ΩHCHO and ΩNO_2 ratio) averaged at each US Drought Monitor (USDM) level. White locations indicate no valid data under a certain USDM level.

3.2. Regional Difference of ΩHCHO and ΩNO_2

To investigate the concurrent changes of O_3 precursors, we compared the spatial maps of ΩHCHO and ΩNO_2 with early afternoon (13:00–14:00) O_3 to match with the overpass time of OMI in Figures 3a–3c. The relative changes from non-drought conditions are shown in Figure S3 in Supporting Information S1. The early afternoon O_3 changes spatially match well with those of MDA8 O_3. ΩHCHO over the southeastern US is the highest, ranging from $\sim 1.2 \times 10^{16}$ to $\sim 1.9 \times 10^{16}$ molec/cm^2, compared with other regions with values of less than 1.0×10^{16} molec/cm^2, which implies the highest isoprene emissions therein. ΩHCHO in the southeastern region also increases with dryness levels. In comparison, ΩNO_2 has little spatial differences with the values staying at $\sim 2.0 \times 10^{15}$ molec/cm^2, except for some relatively higher values over large urban centers (e.g., Los Angeles, New York, and Philadelphia).

As the relative abundance of VOC and NO_x determines the O_3 chemistry mechanism, the ΩHCHO to ΩNO_2 ratio (FNR) has been used to infer whether O_3 formation is VOC-limited or NO_x-limited (Duncan et al., 2010; Jin et al., 2018). High FNR is typically an indicator of NO_x-limited regime and vice versa. Duncan et al. (2010) suggested FNR values of 1 and 2 as thresholds for VOC-limited (FNR < 1), NO_x-limited (FNR > 2), and transition (1 < FNR < 2) regimes and found most of the US were under NO_x-limited regime with the exception of large cities. Recent studies have found that the transition line between the two regimes is uncertain and changes with location (Jin et al., 2017; Schroeder et al., 2017; Souri et al., 2020). Figure 3d displays the FNR at each drought level. The spatial distribution of FNR largely follows that of ΩHCHO, with the highest values of ~6 located in the southeastern US compared with the values of less than four in other areas. This indicates the regional difference of O_3 photochemical regimes, with the southeastern US being the most NO_x-limited area. Similar to ΩHCHO, FNR in the southeast also increases with USDM.

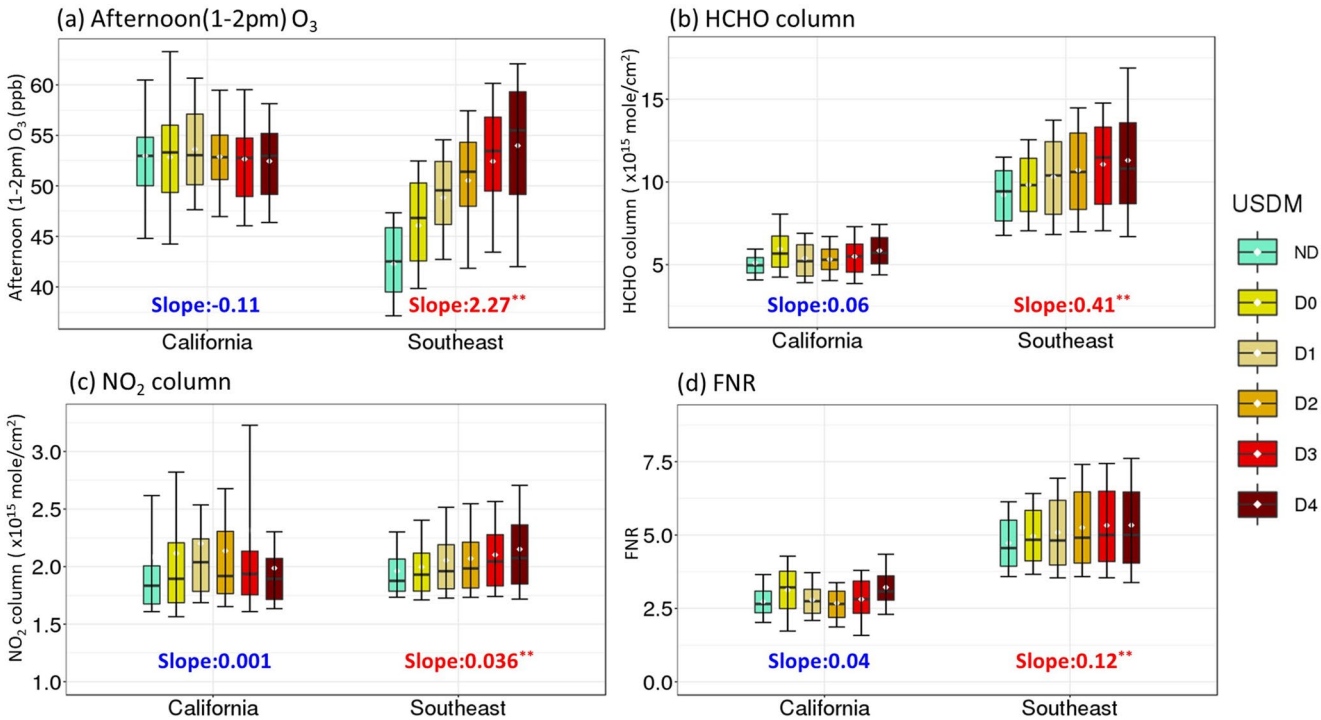

Figure 4. Boxplots of early afternoon O_3 (a), ΩHCHO (b), ΩNO_2 (c), and FNR (d). Slopes and the associated star marks are the same as in Figure 1.

Figure 4 compares the distributions of each variable by USDM between the two regions, with their means and standard deviations listed in Table S2 in Supporting Information S1 and visualized in Figure 5 to better illustrate the variations. ΩHCHO in the southeast is about twice of that in California (Figure 4b), while ΩNO_2 is comparable, with an average value of ~2 × 10^{15} molec/cm^2 among all USDM levels in the two regions (Figure 4c). The high ΩNO_2 standard deviations in California can be attributable to the high agricultural soil NO_x emissions in some areas (e.g., Central Valley). The increasing rate of ΩHCHO and ΩNO_2 with drought severity in the southeast is about 0.41 × 10^{15} molec/cm^2/USDM and 0.036 × 10^{15} molec/cm^2/USDM, respectively. Compared with ND, mean ΩHCHO (ΩNO_2) in this area increased by 6.52%–22.82% (5.26%–10.52%) under D0–D4. Naimark

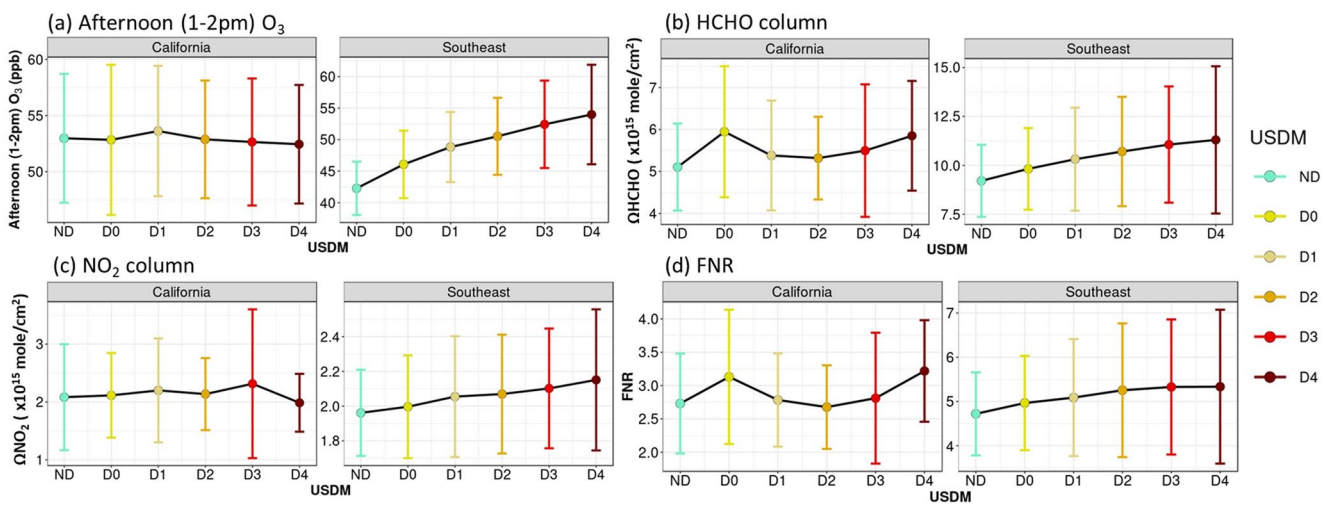

Figure 5. Mean (filled dots) and standard deviation (vertical lines) of early afternoon surface O_3 (a), tropospheric HCHO column (b), NO_2 column (c), and FNR (d) change with US Drought Monitor levels in California and the southeastern US. Note the two regions have different *y*-axis. Detailed data for this figure is shown in Table S2 in Supporting Information S1.

et al. (2021) also reported an enhanced ΩHCHO under drought, with a comparable percentage of 10% over the southeastern US. By contrast, both ΩHCHO and ΩNO_2 in California increase only under low drought levels (e.g., D0–D1) and then decrease under stronger drought categories (e.g., D2–D3) with no statistically significant change rates with USDM.

Because ΩHCHO has higher between-region differences than NO_2, FNR is dominated by ΩHCHO, with a higher mean value in the Southeast (~6) than that in California (~2) (Figure 4d). Furthermore, FNR in the southeast also increases at a rate of 0.12 per USDM due to a faster increasing rate of ΩHCHO than ΩNO_2, which indicates O_3 becomes more NO_x-limited with drought severity in this region. However, there is no statistically significant rate of change for FNR in California, implying an inconsistent change of O_3 regime with drought severity therein.

3.3. Regional Difference of O_3 Chemistry

Using satellite-based FNR as the indicator, we showed in the previous section the regional difference of O_3 chemistry under drought conditions. Here we further quantify the chemistry difference by applying the LaRC zero-dimensional model. We selected three surface sites from California and the southeast, respectively, and each site has at least 10-year data records of VOCs and NO_x observations to ensure at least one weekly observation is available at each USDM level. The site locations are shown in Figure 6a, and more information is provided in Table S1 in Supporting Information S1. The hourly measurements at the three sites were averaged to form "one site" in each region to better represent the regional-mean conditions.

We ran the LaRC zero-dimensional model at each hour and analyzed the averaged results across the daytime hours (9:00–17:00) when photochemistry is most active. As VOCs and NO_x are the most important constraints of the model, we first compared the daytime-mean isoprene, NO_2, and NO at each USDM level in Figures 6b–6d and Table S2 in Supporting Information S1. Isoprene in California generally increases from ND to D1 or D2 and then drops with increasing drought severity. This nonlinear pattern is consistent with both the satellite HCHO in Figure 4b and the previously reported response of isoprene to drought stress (Demetillo et al., 2019; Potosnak et al., 2014; Wang et al., 2017). The largest decrease of isoprene from ND is ~37% at D4. In Georgia, isoprene increases from ND to D1, then drops from D1 to D3, and increases again from D3 to D4. The increase at D4 is about ~41% relative to ND. The detailed time series of the JJA weekly mean isoprene is shown in Figure S4 in Supporting Information S1. In Georgia, D4 only occurred in 2007 at the three sites, while D3 happened in both 2007 and 2012. Drought in 2012 was more widespread and extended for a longer time than that in 2007 (Rippey, 2015). The different behavior of isoprene indicates the complexity of the isoprene response to drought, which depends both on the severity and duration of the drought events. If we define severe drought as when USDM levels are continuously under D2-D4, severe droughts have different features between the southeast and west (Figure S5 in Supporting Information S1); they last longer in the west but occur with a much larger frequency in the south/southeast. Once the western US is stricken by severe droughts, it takes a longer time to recover. That may explain the opposite responses of isoprene to severe drought between California and Georgia.

Similar to ΩNO_2, surface NO_2 shows no clear pattern with drought in California and a slightly increasing pattern in Georgia. NO remains stable at ~1 ppb in both regions across all USDM levels, except for a high value of ~2 ppb at D0 in California. The weekly time series of NO in Figure S6 in Supporting Information S1 show that this abnormal value is mainly caused by the high concentrations at the Clovis and Shafter sites in summer 2018, when the large Ferguson wildfire happened nearby (Mueller et al., 2020). The higher frequency of wildfires in California also makes NO much more variable than that in Georgia. NO_2 does not show high values under D0, possibly because of the high NO:NO_2 ratio in fresh smoke plumes (Juncosa Calahorrano et al., 2021; Selimovic et al., 2018). Furthermore, NO_x has large anthropogenic sources and decreased significantly during our study period, especially at the suburban and urban sites (Figure S6 in Supporting Information S1). This decreasing trend could confound the NO_x changes with USDM, considering drought is not evenly distributed by time. To test whether the NO_x trends significantly affect PO_3 calculated by the zero-dimensional model, we conducted a sensitivity test by fixing NO concentrations at ND for the entire simulation, referred to as fix_NO runs, and the results are shown below and related discussions.

VOCR is used to measure the reactivity of VOCs with OH in the atmosphere. The oxidation of VOCs fuels the O_3 formation by providing peroxy radicals (HO_2 + RO_2), which subsequently react with NO and form NO_2 (cf. Figure 7b). VOCR is derived by the sum of the product of the rate constant for the reaction of each model input

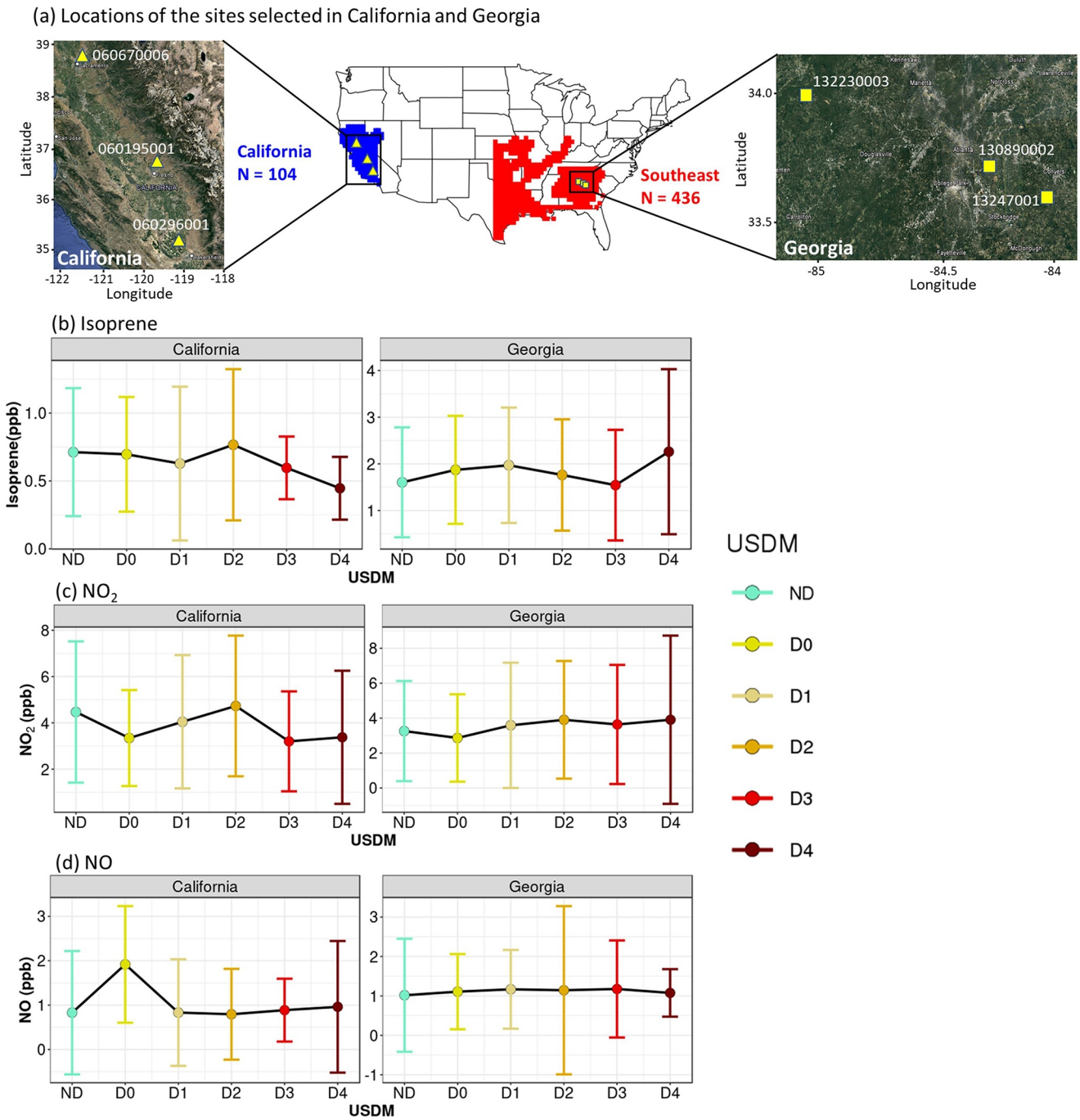

Figure 6. (a) Map of the grids for California (blue) and the southeast US (red) with *N* indicating the number of grids in each region. Yellow dots show the locations of the six sites selected for running the zero-dimensional model in each region with their Air Quality System ID numbers marked below (b)–(d) Mean (filled dots) and standard deviation (vertical lines) of isoprene (b), NO_2 (c), and NO (d) at each US Drought Monitor level calculated from the three sites in California and Georgia, respectively. Detailed data for this figure is shown in Table S1-2 in Supporting Information S1.

VOC with OH multiplied by its concentration. Figure 7a compares the modeled mean of VOCR in the daytime hours. Isoprene and HCHO have the dominant contributions to VOCR in both regions, and they largely control the VOCR changes with USDM. The correlation coefficients (*R*) of VOCR with isoprene are 0.97 and 0.99 in California and Georgia, respectively. Thus, the VOCR changes with drought follow the same pattern of isoprene, with a decrease by up to ~33% in California and an increase by ~36% in Georgia under D4.

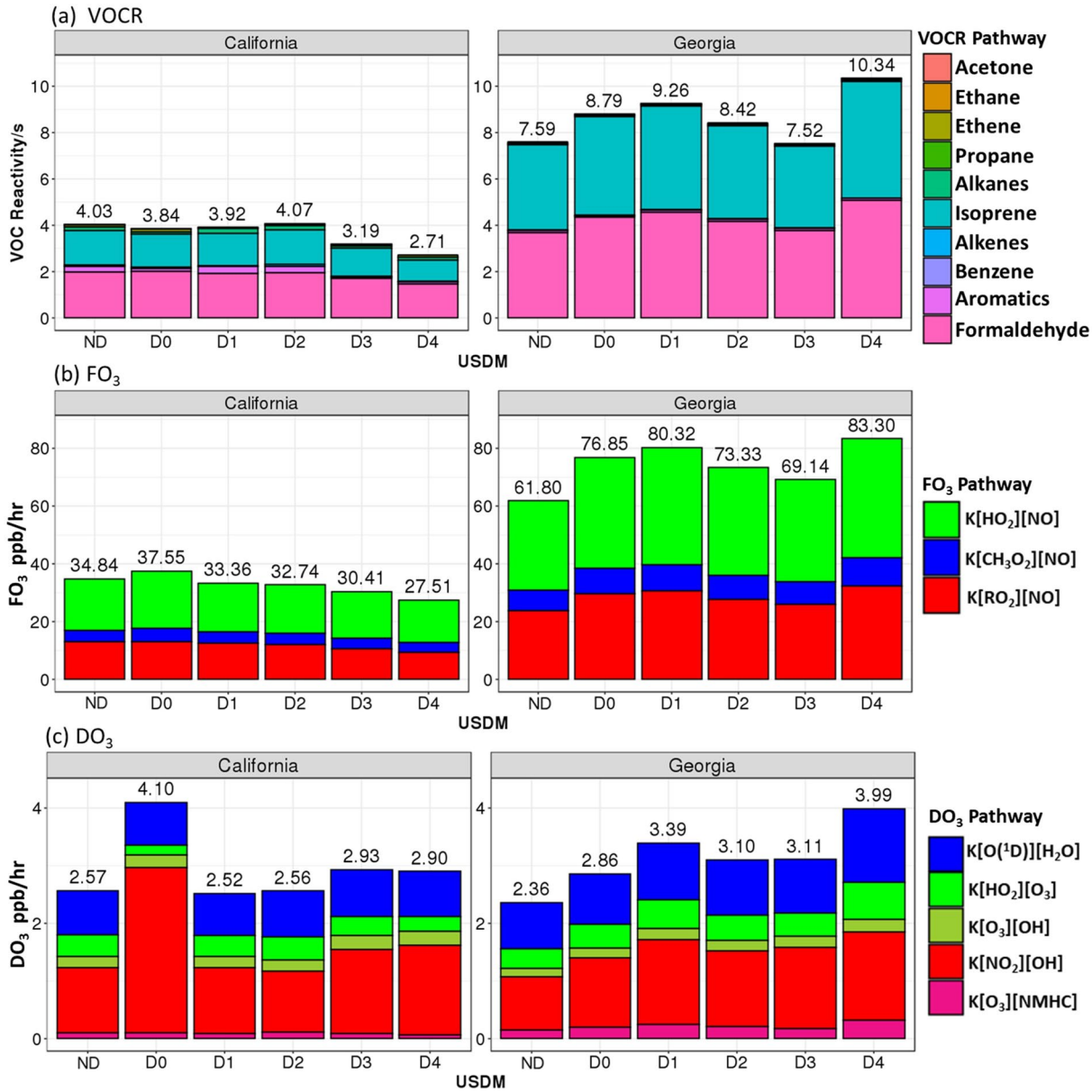

Figure 7. The daytime mean of the total VOC reactivity (a), FO_3 (b), and DO_3 (c) color-coded by their pathways by US Drought Monitor in two regions. The numbers at the top of each bar show the total values.

Figures 7b and 7c illustrate the changes of FO_3 and DO_3 with USDM in the two regions, respectively. Here FO_3 is the sum of the rates of all reactions that convert NO to NO_2 without consuming O_3. Reactions of peroxy radicals with NO have the highest contributions to FO_3. Thus, FO_3 changes with drought are mainly driven by VOCR with a high R value of 0.82 in California and 0.92 in Georgia. ΔFO_3 under D0–D4 ranges from −7.4–2.7 ppb/hr (−21%–7.8%), and 7.3–21.5 ppb/hr (11.8%–34.7%) in California and Georgia, respectively. DO_3 is the sum of all reactions that remove O_x and is mainly driven by NO_2 reaction with OH and O (^{1}D) reaction with water vapor after O_3 photolysis. The highest ΔDO_3 is ∼1.53 ppb/hr under D0 in California, nearly offsetting half of ΔFO_3. Overall ΔDO_3 has small values compared with ΔFO_3, thus contributing little to the changes of PO_3.

Based on the understanding of the FO_3 and DO_3 changes with drought, we further compared the daytime-mean PO_3 by USDM levels. To better illustrate the between-region difference of the O_3 chemistry regime, Figure 8a shows PO_3 changes as a function of NO alone with VOCs held constant at each USDM level (ND-D4). NO is diurnally constant but changes from 0 to 10 ppb with an increment of 0.05 ppb, which is similar to the method

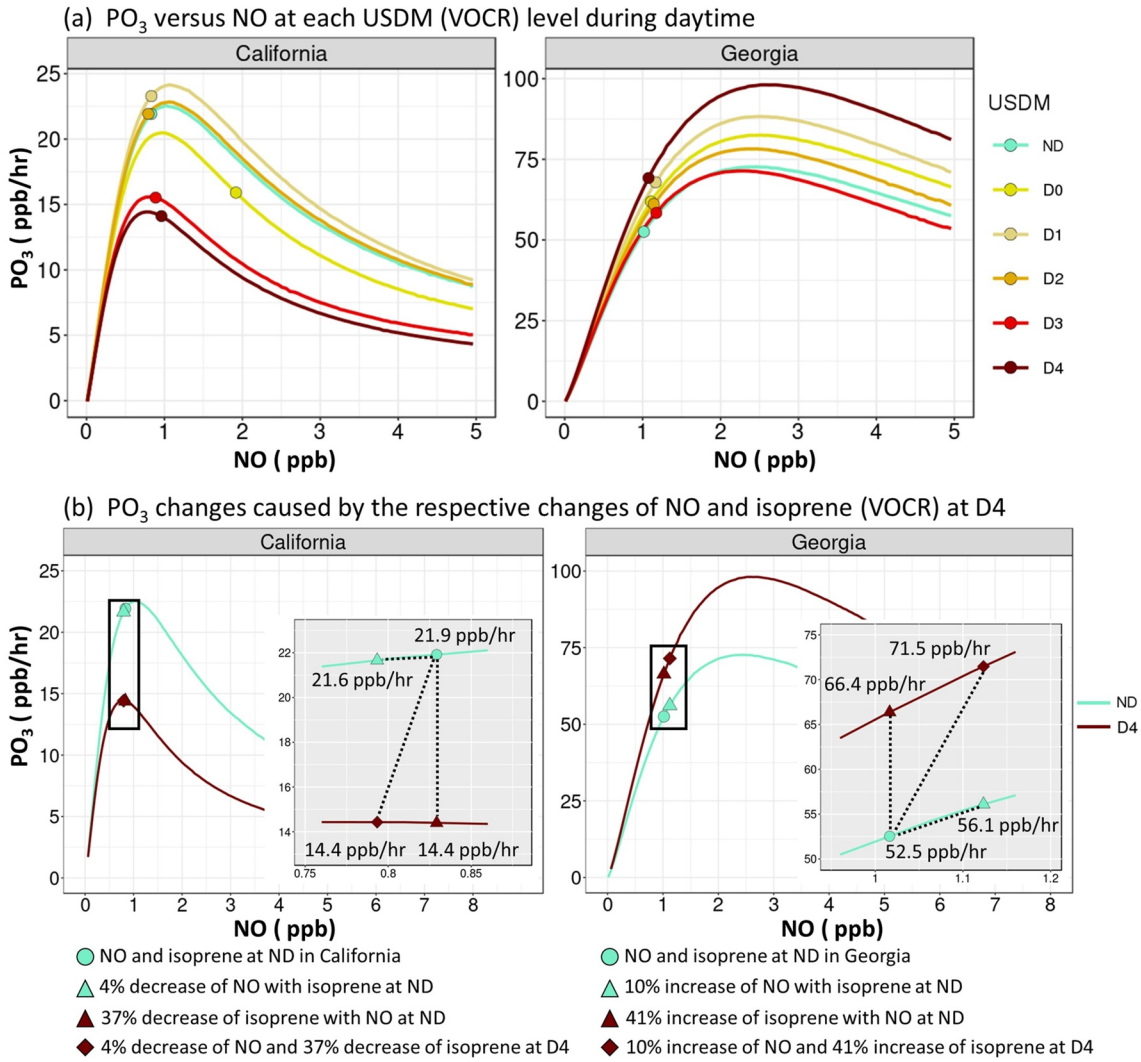

Figure 8. (a) Daytime (9:00–17:00) mean of PO_3 versus NO at the lines of constant VOC reactivity of each US Drought Monitor (USDM) level. NO is diurnally constant but varies from 0 to 10 ppb with an increment of 0.05 ppb. Points highlight the PO_3 values of the USDM-averaged NO observations in each region. (b) Comparison of the PO_3 changes from non-drought (ND) under respective changes of NO and/or isoprene at D4 in California and Georgia. The percentage change of NO is derived from the satellite column data as shown in Figures 4 and 5. The insets (gray background) show the zoom-in views of the main figures covered by the two black boxes. The numbers in the insets indicate the PO_3 values of each point.

used by Schroeder et al., (2017). The filled dots indicate the PO_3 values corresponding to the daytime-mean NO values at each USDM level. Although both regions are under a NO_x-limited regime, California is closer to the regime turning point than Georgia, indicating that O_3 in Georgia is more sensitive to NO_x than that in California, which is consistent with the FNR. As isoprene decreases with drought in California, the O_3 regime shifts to less NO_x-limited or even VOC-limited, leading to a decrease of PO_3 with increasing drought severity. In Georgia, the O_3 regime becomes more NO_x-limited as isoprene increases with drought severity. This is indicated by the higher slopes ($\Delta PO_3/\Delta NO$) of the lines before the regime-turning point as drought severity increases. For example, $\Delta PO_3/\Delta NO$ increased by ~13.41/hr (37%) under D4 relative to ND, whereas the increase is only 8.12/hr (22%) under D1. PO_3 generally follows the increasing pattern of FO_3 in Georgia.

While both regions are in the NO_x-limited regime under non-drought and drought conditions, the much larger relative change of isoprene than NO is the key factor to explain the PO_3 changes from non-drought to drought. To better explain this, we compared the relative changes of PO_3 from ND to D4 due to the respective changes of isoprene and NO separately and in combination. The results are shown in Figure 8b. The PO_3-NO curve calculated using ND and D4 isoprene concentrations is light blue and dark red, respectively. In Georgia, the maximum

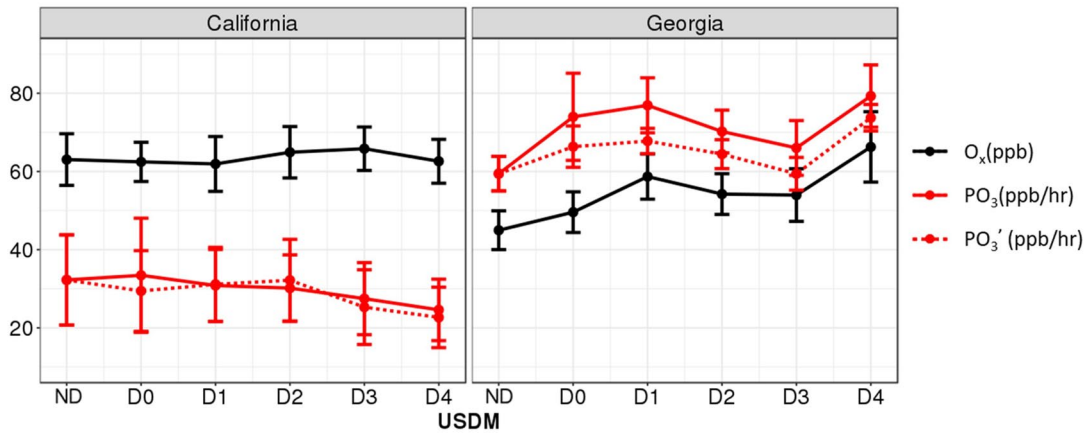

Figure 9. NO observations constrained model results of O_x (black solid line), PO_3 (red solid line), and PO_3' (red dashed line) changes with US Drought Monitor during daytime hours.

increase of NO from non-drought to D4 drought is 10%, derived by satellite NO_2 columns (Figure 4c), while the corresponding increase of isoprene is 41%, derived by surface sites. Non-drought PO_3 is 52.5 ppb/hr (filled blue circle); D4 PO_3 is 71.5 ppb/hr (filled red diamond). Note both points are on the left side of the curve before the turning point, meaning PO_3 is in the NO_x-limited regime. From ND to D4, the 10% increase of NO alone causes PO_3 to increase by ~3.5 ppb/hr (7%) to 59.1 ppb/hr (filled blue triangle), the 41% increase of isoprene leads to an increase of PO_3 by ~13.8 ppb/hr (26%) to 66.4 ppb/hr (filled red triangle), and the increase of both NO and isoprene results in an increase of PO_3 by ~18.9 ppb/hr (36%) to 71.5 ppb/hr (filled red diamond). This breakdown demonstrates that the change of isoprene from ND to D4 contributes 72% of the PO_3 increase while that of NO is only 19%. Similarly, the 4% decrease of NO in California (Figure 4c) results in a decrease of PO_3 by ~0.3 ppb/hr (1%), while the 37% decrease of isoprene causes a reduction of PO_3 by ~7.5 ppb/hr (34%). The decrease of both NO and isoprene leads to a comparable change of PO_3 by ~7.5 ppb/hr. This indicates that the reduction of isoprene can explain almost all the changes of PO_3 in California because the O_3 regime has shifted to the turning point and becomes insensitive to NO. In summary, the much larger relative changes of isoprene than NO is the key driver of the PO_3 changes during drought in both regions.

Figure 9 compares the changes of O_x and PO_3 with USDM levels and their means and standard deviations are listed in Table S2 in Supporting Information S1. The net O_3 production rates from the fix_NO runs are also presented, denoted as PO_3'. Because ND is much more frequent than D0–D4, the fix_NO runs can better represent the average level of NO during the study period. The differences between PO_3 and PO_3' range from ~1% (D1) to ~12% (D0) in California and from ~7% (D4) to ~11% (D1) in Georgia with a respective average value of ~3% and ~8%. The higher difference in Georgia can be explained by its more NO_x-limited regime as illustrated above. Despite the mean offset between PO_3 and PO_3', their variations with USDM levels are similar in both California and Georgia, which indicates the NO_x trend does not significantly affect the results. This similar pattern between PO_3 and PO_3' also consolidates that the considerable change of isoprene and VOCR are the main factors causing the changes of PO_3, although the NO_x-limited regime is dominant in both regions. Compared to ND in the respective region, ΔPO_3 under D4 is 23.7% lower in California but 33.4% higher in Georgia. This difference in the PO_3 response to drought explains the different responses of O_3 to drought between the two regions.

Figure 9 also shows that the relative change of PO_3 with USDM does not explain all of the relative changes of O_x in both regions. For example, in California, PO_3 decreases 10.5% from D3 to D4, but O_x decreases only 4.4%. In Georgia, the increase in O_x from ND to D4 is 46.7%, compared to 33.4% of PO_3. The discrepancies are expected because processes other than chemistry also contribute to the increase of O_3 under drought. A possible non-chemical process facilitating O_3 enhancement under drought is the reduction of O_3 dry deposition. Modeling studies demonstrated that stomatal closure caused by water stress is the major pathway to reduce O_3 dry deposition rates and consequently O_3 concentrations increase during drought (Huang et al., 2016; Kavassalis & Murphy, 2017; Lin et al., 2019). Clifton et al. (2017) and Lin et al. (2019) found a nearly 50% change of dry deposition in summer between drought and non-drought years using observations over the US and Europe. However, the measurements

of dry deposition are scarce and mostly short-term in the CONUS, which limits long-term and between-region analysis.

In conclusion, the different responses of isoprene to drought cause the opposite changes of VOCR and PO_3 between the west and southeast, and consequently explains the east-west spatial contrast of O_3 changes under drought. The different isoprene responses might be attributable to the between-region differences of drought events: longer durations of severe droughts in the west than those in the east.

4. Conclusions

We demonstrated the spatial distributions of O_3 responses to drought over the CONUS using gridded O_3 observations and weekly USDM as drought severity indicator, and found a clear east-west disparity: high O_3 enhancement in the southeast and little change or even decrease in the west. The further between-region analysis shows that the southeast has a statistically significant rate of increase in MDA8 O_3, $\Omega HCHO$, ΩNO_2 and FNR with USDM levels, with the corresponding rate of 2.24 ppb/USDM, 0.41×10^{15} molec/cm^2/USDM, 0.03×10^{15} molec/cm^2/USDM and 0.12/USDM. These variables do not show a statistically significant changing rate with USDM in California. Diurnal ΔO_3 also shows opposite patterns between the southeast and California.

The zero-dimensional model results revealed the O_3 chemistry differences caused by the opposite responses of isoprene to drought between the southeast and west. The daytime decrease of O_3 under drought in California is attributable to the up to ~23.7% reduction of the O_3 production rate (PO_3) due to a ~37% decrease of isoprene emissions. On the contrary, isoprene increased by ~41% at D4 in Georgia, causing a consequent increase of PO_3 by ~33.4% which accounts for more than half of the O_3 increase under drought. We further showed that the changes of isoprene under drought resulted in changes in the sensitivity of the O_3 chemistry to NO_x. In the southeastern region, the increase of isoprene makes O_3 more sensitive to NO_x. Thus, to achieve the same O_3 air quality under drought in this region would require a more stringent control of anthropogenic NO_x emissions and a better characterization of natural soil NO_x emissions changes. In California, the reduced isoprene makes O_3 less sensitive to NO_x. Under this scenario, O_3 formation could even become VOC-limited under D4 (Figure 8a), which could partly offset or reverse the benefits of the NO_x emission control under severe drought conditions.

The opposite drought-isoprene changes between California and the southeast US are likely due to the different responses of plants to water stress partly controlled by the duration of the drought period. During short-term or mild droughts, isoprene emissions are not immediately impacted because of the availability of stored carbon and because photosynthetic electron transport is not inhibited. Isoprene can even increase by several factors due to warm leaf temperatures which increases isoprene synthase activity (Guenther et al., 2017). This explains the general trend of isoprene increasing with drought in the southeast US. During longer severe water stress, isoprene emission eventually declines because of inadequate carbon availability caused by reduced photosynthesis (Potosnak et al., 2014). The absence of isoprene increase with drought in California indicates plants are in this stage even during a mild drought. As the summer season in California typically receives little rainfall (Mediterranean climate), it is likely plants in California are under chronic water stress in summer under non-drought conditions. A mild drought could quickly trigger severe water stress to terrestrial plants and as a result, isoprene emissions are immediately impacted by drought-triggered inhibition of photosynthetic electron transport or lack of stored carbon. While BVOC emission models such as MEGAN predict reduced isoprene emissions under severe drought, they do not capture the spatial differences (Emmerson et al., 2019; Jiang et al., 2018) and underestimated isoprene concentrations during mild or moderate drought (Potosnak et al., 2014; Seco et al., 2015). Our results suggest that drought duration, in addition to drought severity, should also be included in the model algorithm development.

Although PO_3 changes could explain more than half of O_3 changes during drought, O_3 chemistry alone is not enough to fully account for the relative changes of O_3 due to the contributions from other non-chemical processes such as dry deposition. Dry deposition is a possible non-chemical process to explain the O_3 changes during drought. The scarcity of dry deposition observations in the CONUS makes it a challenge to conduct a long-term between-region comparison of dry deposition-O_3 relationships. There are ongoing modeling developments in O_3 dry deposition parameterization that is coupled with vegetation and land models to consider dynamic terrestrial-atmosphere interactions (Anav et al., 2018; Clifton et al., 2020; Gong et al., 2020; Lin et al., 2019; Wong et al., 2019), which will make it possible to simulate the dry deposition changes under drought. As drought is predicted to become more frequent in the future (Cook et al., 2018; Coumou & Rahmstorf, 2012), it will require

more long-term observations of isoprene emissions and O_3 dry deposition rates during different drought phases to improve our understanding and predictive ability of the process-driven drought-O_3 coupling.

Data Availability Statement

The data used for this study are available online (at https://doi.org/10.7910/DVN/CKX4RP).

Acknowledgments
This research was supported in part by the NOAA's Atmospheric Chemistry, Carbon Cycle, and Climate (AC4) Program (NA19OAR4310177). It was also supported by NASA Atmospheric Composition Modeling and Analysis Program (80NSSC19K0986). The authors acknowledge EPA for providing the hourly observations of trace gases and meteorological parameters for running the LaRC zero-dimensional model, NASA Langley Research Center for the OMI NO_2 and HCHO column data. We thank the National Drought Mitigation Center for making and providing the USDM maps.

References

Abeleira, A. J., & Farmer, D. K. (2017). Summer ozone in the northern front range metropolitan area: Weekend–weekday effects, temperature dependences, and the impact of drought. *Atmospheric Chemistry and Physics*, *17*(11), 6517–6529. https://doi.org/10.5194/acp-17-6517-2017

Anav, A., Proietti, C., Menut, L., Carnicelli, S., De Marco, A., & Paoletti, E. (2018). Sensitivity of stomatal conductance to soil moisture: Implications for tropospheric ozone. *Atmospheric Chemistry and Physics*, *18*(8), 5747–5763. https://doi.org/10.5194/acp-18-5747-2018

Brilli, F., Barta, C., Fortunati, A., Lerdau, M., Loreto, F., & Centritto, M. (2007). Response of isoprene emission and carbon metabolism to drought in white poplar (Populus alba) saplings. *New Phytologist*, *175*(2), 244–254. https://doi.org/10.1111/j.1469-8137.2007.02094.x

Chen, L. G., Gottschalck, J., Hartman, A., Miskus, D., Tinker, R., & Artusa, A. (2019). Flash drought characteristics based on U.S. drought monitor. *Atmosphere*, *10*(9), 498. https://doi.org/10.3390/atmos10090498

Clifton, O. E., Fiore, A. M., Munger, J. W., Malyshev, S., Horowitz, L. W., Shevliakova, E., et al. (2017). Interannual variability in ozone removal by a temperate deciduous forest. *Geophysical Research Letters*, *44*(1), 542–552. https://doi.org/10.1002/2016GL070923

Clifton, O. E., Paulot, F., Fiore, A. M., Horowitz, L. W., Correa, G., Baublitz, C. B., et al. (2020). Influence of dynamic ozone dry deposition on ozone pollution. *Journal of Geophysical Research: Atmospheres*, *125*(8). https://doi.org/10.1029/2020JD032398

Cook, B. I., Mankin, J. S., & Anchukaitis, K. J. (2018). Climate change and drought: From past to future. *Current Climate Change Reports*, *4*(2), 164–179. https://doi.org/10.1007/s40641-018-0093-2

Coumou, D., & Rahmstorf, S. (2012). A decade of weather extremes. *Nature Climate Change*, *2*(7), 491–496. https://doi.org/10.1038/nclimate1452

Crawford, J., Davis, D., Olson, J., Chen, G., Liu, S., Gregory, G., et al. (1999). Assessment of upper tropospheric HOx sources over the tropical Pacific based on NASA GTE/PEM data: Net effect on HOx and other photochemical parameters. *Journal of Geophysical Research: Atmospheres*, *104*(D13), 16255–16273. https://doi.org/10.1029/1999JD900106

Demetillo, M. A. G., Anderson, J. F., Geddes, J. A., Yang, X., Najacht, E. Y., Herrera, S. A., et al. (2019). Observing severe drought influences on ozone air pollution in California. *Environmental Science & Technology*, *53*(9), 4695–4706. https://doi.org/10.1021/acs.est.8b04852

Duncan, B. N., Yoshida, Y., Olson, J. R., Sillman, S., Martin, R. V., Lamsal, L., et al. (2010). Application of OMI observations to a space-based indicator of NOx and VOC controls on surface ozone formation. *Atmospheric Environment*, *44*(18), 2213–2223. https://doi.org/10.1016/j.atmosenv.2010.03.010

Emmerson, K. M., Palmer, P. I., Thatcher, M., Haverd, V., & Guenther, A. B. (2019). Sensitivity of isoprene emissions to drought over south-eastern Australia: Integrating models and satellite observations of soil moisture. *Atmospheric Environment*, *209*, 112–124. https://doi.org/10.1016/j.atmosenv.2019.04.038

Flynn, J., Lefer, B., Rappenglück, B., Leuchner, M., Perna, R., Dibb, J., et al. (2010). Impact of clouds and aerosols on ozone production in Southeast Texas. *Atmospheric Environment*, *44*(33), 4126–4133. https://doi.org/10.1016/j.atmosenv.2009.09.005

Gong, C., Lei, Y., Ma, Y., Yue, X., & Liao, H. (2020). Ozone–vegetation feedback through dry deposition and isoprene emissions in a global chemistry–carbon–climate model. *Atmospheric Chemistry and Physics*, *20*(6), 3841–3857. https://doi.org/10.5194/acp-20-3841-2020

Guenther, A. B., Shah, T., & Huang, L. (2017). *A next generation modeling system for estimating Texas biogenic VOC emissions [M]* (pp. 16-011). AQRP Project.

Guo, F., Bui, A. A. T., Schulze, B. C., Yoon, S., Shrestha, S., Wallace, H. W., et al. (2021). Urban core-downwind differences and relationships related to ozone production in a major urban area in Texas. *Atmospheric Environment*, *262*, 118624. https://doi.org/10.1016/j.atmosenv.2021.118624

Heim, R. R. (2002). A review of twentieth-century drought indices used in the United States. *Bulletin of the American Meteorological Society*, *83*(8), 1149–1166. https://doi.org/10.1175/1520-0477-83.8.1149

Horton, D. E., Skinner, C. B., Singh, D., & Diffenbaugh, N. S. (2014). Occurrence and persistence of future atmospheric stagnation events. *Nature Climate Change*, *4*(8), 698–703. https://doi.org/10.1038/nclimate2272

Huang, L., McDonald-Buller, E. C., McGaughey, G., Kimura, Y., & Allen, D. T. (2016). The impact of drought on ozone dry deposition over eastern Texas. *Atmospheric Environment*, *127*, 176–186. https://doi.org/10.1016/j.atmosenv.2015.12.022

Jiang, X., Guenther, A., Potosnak, M., Geron, C., Seco, R., Karl, T., et al. (2018). Isoprene emission response to drought and the impact on global atmospheric chemistry. *Atmospheric Environment*, *183*, 69–83. https://doi.org/10.1016/j.atmosenv.2018.01.026

Jin, X., Fiore, A. M., & Geigert, M. (2018). *Using satellite observed formaldehyde (HCHO) and nitrogen dioxide (NO_2) as an indicator of ozone sensitivity in a SIP*. https://doi.org/10.7916/D8M34C7V

Jin, X., Fiore, A. M., Murray, L. T., Valin, L. C., Lamsal, L. N., Duncan, B., et al. (2017). Evaluating a space-based indicator of surface ozone-NOx-VOC sensitivity over midlatitude source regions and application to decadal trends. *Journal of Geophysical Research: Atmospheres*, *122*(1910), 439461–439510. https://doi.org/10.1002/2017JD026720

Juncosa Calahorrano, J. F., Lindaas, J., O'Dell, K., Palm, B. B., Peng, Q., Flocke, F., et al. (2021). Daytime oxidized reactive nitrogen partitioning in western U.S. Wildfire smoke plumes. *Journal of Geophysical Research: Atmospheres*, *126*(4). https://doi.org/10.1029/2020JD033484

Kaiser, J., Jacob, D. J., Zhu, L., Travis, K. R., Fisher, J. A., González Abad, G., et al. (2018). High-resolution inversion of OMI formaldehyde columns to quantify isoprene emission on ecosystem-relevant scales: Application to the Southeast US. *Atmospheric Chemistry and Physics*, *18*(8), 5483–5497. https://doi.org/10.5194/acp-18-5483-2018

Kavassalis, S. C., & Murphy, J. G. (2017). Understanding ozone-meteorology correlations: A role for dry deposition. *Geophysical Research Letters*, *44*(6), 2922–2931. https://doi.org/10.1002/2016GL071791

Lamsal, L. N., Martin, R. V., Donkelaar, A. van, Steinbacher, M., Celarier, E. A., Bucsela, E., et al. (2008). Ground-level nitrogen dioxide concentrations inferred from the satellite-borne Ozone Monitoring Instrument. *Journal of Geophysical Research*, *113*(D16). https://doi.org/10.1029/2007JD009235

Lin, M., Malyshev, S., Shevliakova, E., Paulot, F., Horowitz, L. W., Fares, S., et al. (2019). Sensitivity of ozone dry deposition to ecosystem-atmosphere interactions: A critical appraisal of observations and simulations. *Global Biogeochemical Cycles*, *33*(10), 1264–1288. https://doi.org/10.1029/2018GB006157

McKee, T. B., Doesken, N. J., & Kleist, J. (1993). *The relationship of drought frequency and duration to time scales*.

Mueller, S., Tarnay, L., O'Neill, S., & Raffuse, S. (2020). Apportioning smoke impacts of 2018 wildfires on eastern Sierra Nevada sites. *Atmosphere*, *11*(9), 970. https://doi.org/10.3390/atmos11090970

Naimark, J. G., Fiore, A. M., Jin, X., Wang, Y., Klovenski, E., & Braneon, C. (2021). Evaluating drought responses of surface ozone precursor proxies: Variations with land cover type, precipitation, and temperature. *Geophysical Research Letters*, *48*(7). https://doi.org/10.1029/2020GL091520

Olson, J. R., Crawford, J. H., Chen, G., Brune, W. H., Faloona, I. C., Tan, D., et al. (2006). A reevaluation of airborne HOx observations from NASA field campaigns. *Journal of Geophysical Research*, *111*(D10). https://doi.org/10.1029/2005JD006617

Otkin, J. A., Svoboda, M., Hunt, E. D., Ford, T. W., Anderson, M. C., Hain, C., & Basara, J. B. (2018). Flash droughts: A review and assessment of the challenges imposed by rapid-onset droughts in the United States. *Bulletin of the American Meteorological Society*, *99*(5), 911–919. https://doi.org/10.1175/BAMS-D-17-0149.1

Pegoraro, E., Rey, A., Barron-Gafford, G., Monson, R., Malhi, Y., & Murthy, R. (2005). The interacting effects of elevated atmospheric CO2 concentration, drought and leaf-to-air vapour pressure deficit on ecosystem isoprene fluxes. *Oecologia*, *146*(1), 120–129. https://doi.org/10.1007/s00442-005-0166-5

Potosnak, M. J., LeStourgeon, L., Pallardy, S. G., Hosman, K. P., Gu, L., Karl, T., et al. (2014). Observed and modeled ecosystem isoprene fluxes from an oak-dominated temperate forest and the influence of drought stress. *Atmospheric Environment*, *84*, 314–322. https://doi.org/10.1016/j.atmosenv.2013.11.055

Rippey, B. R. (2015). The U.S. drought of 2012. *Weather and Climate Extremes*, *10*, 57–64. https://doi.org/10.1016/j.wace.2015.10.004

Schnell, J. L., Holmes, C. D., Jangam, A., & Prather, M. J. (2014). Skill in forecasting extreme ozone pollution episodes with a global atmospheric chemistry model. *Atmospheric Chemistry and Physics*, *14*(15), 7721–7739. https://doi.org/10.5194/acp-14-7721-2014

Schroeder, J. R., Crawford, J. H., Fried, A., Walega, J., Weinheimer, A., Wisthaler, A., et al. (2017). New insights into the column CH2O/NO2 ratio as an indicator of near-surface ozone sensitivity. *Journal of Geophysical Research: Atmospheres*, *122*(16), 8885–8907. https://doi.org/10.1002/2017JD026781

Seco, R., Karl, T., Guenther, A., Hosman, K. P., Pallardy, S. G., Gu, L., et al. (2015). Ecosystem-scale volatile organic compound fluxes during an extreme drought in a broadleaf temperate forest of the Missouri Ozarks (central USA). *Global Change Biology*, *21*(10), 3657–3674. https://doi.org/10.1111/gcb.12980

Selimovic, V., Yokelson, R. J., Warneke, C., Roberts, J. M., de Gouw, J., Reardon, J., & Griffith, D. W. T. (2018). Aerosol optical properties and trace gas emissions by PAX and OP-FTIR for laboratory-simulated western US wildfires during FIREX. *Atmospheric Chemistry and Physics*, *18*(4), 2929–2948. https://doi.org/10.5194/acp-18-2929-2018

Simon, H., Reff, A., Wells, B., Xing, J., & Frank, N. (2015). Ozone trends across the United States over a period of decreasing NOx and VOC emissions. *Environmental Science & Technology*, *49*(1), 186–195. https://doi.org/10.1021/es504514z

Solberg, S., Hov, Ø., Søvde, A., Isaksen, I. S. A., Coddeville, P., Backer, H. D., et al. (2008). European surface ozone in the extreme summer 2003. *Journal of Geophysical Research*, *113*(D7). https://doi.org/10.1029/2007JD009098

Souri, A. H., Nowlan, C. R., Wolfe, G. M., Lamsal, L. N., Chan Miller, C. E., Abad, G. G., et al. (2020). Revisiting the effectiveness of HCHO/NO2 ratios for inferring ozone sensitivity to its precursors using high resolution airborne remote sensing observations in a high ozone episode during the KORUS-AQ campaign. *Atmospheric Environment*, *224*, 117341. https://doi.org/10.1016/j.atmosenv.2020.117341

Svoboda, M., LeComte, D., Hayes, M., Heim, R., Gleason, K., Angel, J., et al. (2002). The drought monitor. *Bulletin of the American Meteorological Society*, *83*(8), 1181–1190. https://doi.org/10.1175/1520-0477-83.8.1181

Vicente-Serrano, S. M., Beguería, S., & López-Moreno, J. I. (2010). A multiscalar drought index sensitive to global warming: The standardized precipitation evapotranspiration index. *Journal of Climate*, *23*(7), 1696–1718. https://doi.org/10.1175/2009JCLI2909.1

Wang, Y., Xie, Y., Dong, W., Ming, Y., Wang, J., & Shen, L. (2017). Adverse effects of increasing drought on air quality via natural processes. *Atmospheric Chemistry and Physics*, *17*(20), 12827–12843. https://doi.org/10.5194/acp-17-12827-2017

Wong, A. Y. H., Geddes, J. A., Tai, A. P. K., & Silva, S. J. (2019). Importance of dry deposition parameterization choice in global simulations of surface ozone. *Atmospheric Chemistry and Physics*, *19*(22), 14365–14385. https://doi.org/10.5194/acp-19-14365-2019

Yan, Y., Lin, J., & He, C. (2018). Ozone trends over the United States at different times of day. *Atmospheric Chemistry and Physics*, *18*(2), 1185–1202. https://doi.org/10.5194/acp-18-1185-2018

Zhang, Y., & Wang, Y. (2016). Climate-driven ground-level ozone extreme in the fall over the Southeast United States. *Proceedings of the National Academy of Sciences*, *113*(36), 10025–10030. https://doi.org/10.1073/pnas.1602563113

Zhu, L., Mickley, L. J., Jacob, D. J., Marais, E. A., Sheng, J., Hu, L., et al. (2017). Long-term (2005–2014) trends in formaldehyde (HCHO) columns across North America as seen by the OMI satellite instrument: Evidence of changing emissions of volatile organic compounds. *Geophysical Research Letters*, *44*(13), 7079–7086. https://doi.org/10.1002/2017GL073859